Available online at www.sciencedirect.com
ScienceDirect
Journal of Hydrodynamics
2009,21(2):176-189
DOI: 10.1016/S1001-6058(08)60135-3
www.sciencedirect.com/science/journal/10016058

CAVITATION NUCLEI: EXPERIMENTS AND THEORY*

MØRCH K. A.
Department of Physics and Center of Quantum Protein, DK-2800 Kongens Lyngby, Denmark,
E-mail: morch@fysik.dtu.dk

(Received October 18, 2008, Revised December 20, 2008)

Abstract: The Swedish astrophysicist and Nobel Prize winner Hannes Alfvén said: Theories come and go ─ the experiment is here forever. Often a theory, which we set up to describe an observed physical phenomenon, suffers from the lack of knowledge of decisive parameters, and therefore at best the theory becomes insufficient. Contrary, the experiment always reveals nature itself, though at prevailing experimental conditions. With essential parameters being out of control and even maybe unidentified, apparently similar experiments may deviate way beyond our expectations. However, these discrepancies offer us a chance to reflect on the character of the unknown parameters. In this way non-concordant experimental results may hold the key to the development of better theories – and to new experiments for the testing of their validity. Cavitation and cavitation nuclei are phenomena of that character.

Key words: cavitation nuclei, gas bubbles, surface nano voids, scanning tunneling microscopy, atomic force microscopy

Nomenclature

h ─ Height of spherical cap
z ─ Distance along surface normal
A ─ Area of bubble surface
A_{H_2O} ─ Area of pure water on bubble surface
F_{AFM} ─ Force on AFM cantilever
L ─ Length characteristic of body
V ─ Bubble volume
V_s ─ Volume below spherical cap
V_{sph} ─ Volume of spherical cap
Δp ─ Pressure jump across bubble surface
γ_{H_2O} ─ Surface tension of pure water
σ ─ Thoma cavitation number
Φ ─ Barrier height, work function
Γ ─ Contact radius of bubble cap
$crit$ ─ Critical conditions
o ─ Initial conditions (t=0)
$*$ ─ Normalized quantity

* **Biography:** MØRCH K. A., Male, Ph. D., Professor Emeritus

1. Introduction

Homogeneous cavitation in pure water has been calculated theoretically to occur at a tensile stress of ~140 MPa at 25°C[1], and this value has actually been achieved experimentally by isochoric cooling of ultra-pure water trapped in inclusions in quarts[2]. However, at normal conditions water has almost no tensile strength, and even when utmost care is taken to control experimental conditions that may influence its tensile strength, it comes up to only a fraction of the theoretical value. The highest value ever obtained is 27.7 MPa measured by Briggs[3]. In his experiments extreme cleanliness in preparation of the water and the equipment was a decisive factor.

It is apparent that a normal single-phase liquid carries defects, cavitation nuclei, which are decisive for its tensile strength. In this context it is relevant to consider the well-established basic theory of spherical gas-vapour bubbles, which are immediate candidates.

The dynamics of gas/vapour bubbles in a liquid[4] is governed by the Rayleigh-Plesset equation

$$R\frac{\mathrm{d}^2R}{\mathrm{d}t^2}+\frac{3}{2}\left(\frac{\mathrm{d}R}{\mathrm{d}t}\right)^2=\frac{1}{\rho_L}(p_g+p_v-p_\infty-$$

$$\frac{4\mu_L}{R}\frac{\mathrm{d}R}{\mathrm{d}t}-\frac{2\gamma}{R}) \qquad (1)$$

in which R is the bubble radius, ρ_L , μ_L and γ are the density, the dynamic viscosity and the surface tension of the liquid, respectively, p_g is the pressure of the non-condensable gas in the bubble, p_v is the vapour pressure, and p_∞ is the far field pressure, while t is the time. At equilibrium conditions Eq.(1) reduces to

$$p_g+p_v=p_\infty+\frac{2\gamma}{R} \qquad (2)$$

and as a consequence, for given mass m of non-condensable gas in the bubble and at isothermal conditions, equilibrium can be obtained when the far field pressure is above a critical limit

$$p_{\infty,crit}-p_v=-\frac{4\gamma}{3R_{crit}} \qquad (3a)$$

in which

$$R_{crit}=\sqrt{\frac{9mB_sT}{8\pi\gamma}} \qquad (3b)$$

Here B_s is the specific gas constant and T is the absolute temperature. The critical pressure defines the tensile strength *TS* of the liquid due to the bubble by

$$TS=p_v-p_{\infty,crit} \qquad (4)$$

In Fig.1 examples of bubble equilibrium curves in water are shown, calculated from Eq.(2) at different values of *m*. For $R<R_{crit}$ the equilibrium is stable, i.e., the bubble remains in equilibrium at small pressure disturbances, while for $R>R_{crit}$ the equilibrium is unstable. Therefore, when a gas bubble expands beyond R_{crit} it grows explosively into an essentially vaporous cavity. By example, at atmospheric conditions a gas bubble of radius 5 μm gives water a tensile strength of only ~5.3 kPa .

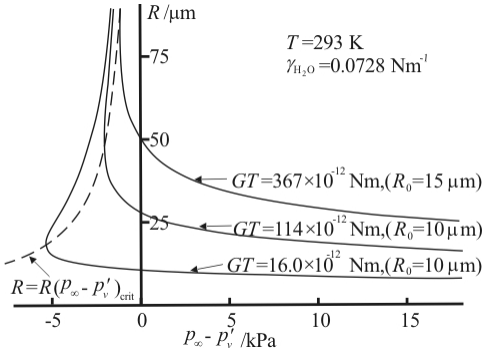

Fig.1 Equilibrium curves for free gas bubbles of different gas content (diffusion of gas is neglected). For $R<R_{crit}$ the gas bubbles are in stable equilibrium, while for $R>R_{crit}$ they grow explosively into vaporous cavities[5]

In the above considerations, diffusion of gas is ignored, but actually, due to diffusion also gas bubbles, which are smaller than their critical size, are inherently unstable, and in water the high surface tension gives micro-bubbles a short lifetime. The excess pressure in the bubbles makes them go into solution at increasing velocity as they shrink in size[6]. Thus, gas bubbles cannot act as cavitation nuclei unless somehow stabilised.

2. Experiments and analysis

Most of the experimental work reported on cavitation inception refers to water, and the present analysis is based primarily on such results. An early observation of cavitation inception was that it usually occurs at solid surfaces bounding the liquid, and Harvey et al.[7] suggested that gas pockets, trapped in hydrophobic conical cracks and crevices of solid surfaces, act as cavitation nuclei. Here a gas pocket may have a negative radius of curvature, which allows it to be stable to gas diffusion. Experiments documented that the tensile strength was increased at pressurization as well as by degassing the liquid[8,9], features that both can be explained from the Harvey-model of cavitation nuclei. However, it seems difficult to explain from this model why the maximum of tensile strength for water occurs at 10°C, and quickly drops towards low values when the temperature approaches 0°C. This maximum was measured in Brigg's experiments with highly cleaned water as well as in Keller's[10] experiments with ordinary tap water, the latter at stress levels two orders of magnitude lower than in Briggs' experiments.

Another model by Fox and Herzfeld considered free gas bubbles in a liquid to be stabilised by a skin

of organic molecules such as fatty acids[11]. The skin was supposed to prevent the bubble from collapsing below some minimum size, and to stop gas diffusion when this size was acquired. However, an organic skin would dissolve in liquids as alcohol and tetrachloride, and these liquids also exhibit cavitation. A revised skin-model by Yount[12,13], the Varying-Permeability (VP) model, assumes the skin to be formed by surface-active (amphiphilic) molecules that allow the gas pressure in the bubble to be in diffusion balance with the gas in solution in the surrounding liquid, and the skin makes the bubble able to resist collapse.

Actually, Johnson and Cooke[14] have documented experimentally that at atmospheric pressure gas bubbles in seawater can be stabilised by a skin. The gas bubbles they produced dissolved at increasing speed as their radius decreased, and some bubbles collapsed completely, but a small transparent remnant was always left, and it was taken to be composed of material that originally was present on the gas-water interface, others stopped their collapse abruptly, apparently being stabilised by a surface film that had contracted during the shrinking of the bubble, until it resisted further collapse. The stabilised gas bubbles were sometimes slightly aspherical and of diameters from less than 1μm (column of histogram 0.75 μm - 2.25 μm) to 13.5 μm, the number density shifting towards the lower size limit by time. At exposure to small tensile stresses the stabilised bubbles expanded, at first slowly, then more rapidly. When the tensile stress was removed most of them reverted to approximately their stabilised size, though some of them dissolved completely. Compressive stress up to 8.3 kPa caused rapid and complete dissolution of some of the stable micro-bubbles, and more of them dissolved, the larger their diameters. Increase of the pressure by up to 13.8 kPa resulted in the collapse of all stabilised bubbles. Likewise, Yount et al.[15] observed stabilised gas bubbles in distilled water, and show a stable binary of bubble radius ~1.5 μm. Did a skin prevent the binary from merging into a single bubble? In agarose gelatine Yount[15] observed stabilised gas bubbles smaller than those observed in water, but the influence of the agarose makes these bubbles unsuited for conclusions in relation to the present analysis.

Johnson and Cooke's experimental results convincingly show that free gas bubbles can be stabilised by a skin. Therefore we can expect such nuclei to be present, in particular in seawater, but also in other liquids, and Yount's VP-model seems a good approach to a description of their stabilisation. However, the question remains, which nuclei are the primary ones for the occurrence of cavitation: free gas bubbles, or gas bubbles attached to solid surfaces? We notice three observations that put limits to the importance on skin-stabilised free gas bubbles:

(1) The size range of the skin stabilised bubbles measured by Johnson and Cooke indicates that these bubbles can be responsible for the tensile strength of water only up to ~0.15 MPa, i.e. very much lower values than those obtained by Briggs, and also notably less than measured by Harvey et al.[7], Strasberg[8], Barger[9], and by Sirotyuk [16] who came up to more than 1 MPa by degassing and cleaning water from surface-active substances as much as possible. Sirotyuk's documentation of the importance of these substances is most important and in harmony with Brigg's observations. His conclusion, that "the stabilisation of gas bubbles, acting as cavitation nuclei, is always attributable to the presence of surface-active substances" may have a broad validity, but only if we take "gas bubbles" to be free gas bubbles as well as interfacial voids at solid surfaces. Having filtered away particles "whose pores and fissures can collect air", i.e., large particles, from his water, Sirotyuk deemed the remaining particles to be without influence, but Greenspan and Tschiegg[17] had shown already that particles of size down to 0.2 μm were decisive for the tensile strength of water, and definitely the interplay of particles with surface-active substances is important.

(2) The collapse of the skin stabilized free gas bubbles observed by Johnson and Cooke at low compressive stress exclude them as the cavitation nuclei surviving in pressurisation experiments up to 100 MPa reported by Harvey et al. and Strasberg.

(3) Finally, skin stabilised free gas bubbles seem unable to explain the maximum of the tensile strength observed at 10°C in highly cleaned water as well as in tap water – but Harvey's original crevice model cannot explain this observation either.

Greenspan and Tschiegg's experiments[17] proved that the tensile strength of distilled water increased when particles were filtered away, the more the smaller the size of the remaining particles, until the largest ones were less than 0.2 μm in diameter. With only such small particles left, the tensile strength came above 10 MPa for an essentially unlimited time, and up to 21 MPa for several seconds in acoustic cavitation experiments at 43 kHz. Surprisingly, at these conditions the gas tension in the water had no influence. Filtering to smaller particle sizes had no measurable effect. These remarkable features seem to be related to the global radius of the particles, their surface shape and character. Convex surface structures strengthen solid/liquid contact while concave structures, surface steps and/or contamination may lead to local detachment of water from solid surfaces[18,19]. Crum[20] shows a typical large particle, filtered away from distilled water, and it exhibits a

rough surface, composed of concave structures of different dimensions, separated by crests, while cracks are not readily identified. Such surface structures may be ideal for the development of neighboring interfacial voids which at low tensile stress merge into larger cavities. Thus the basic concept of cracks and crevices in Harvey's original model is not necessarily the only source of interfacial cavitation nuclei. Contrary, nano-particles are highly convex globally, and Greenspan and Tschiegg's experimental finding that such particles did not cause cavitation inception, indicates that if cavitation nuclei were present at all at local non-convex surface structures they were too small to grow and merge into larger ones.

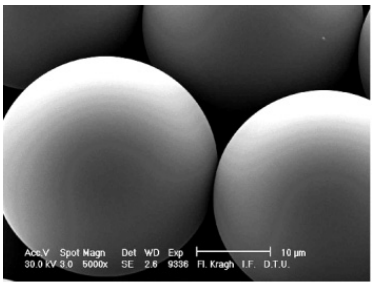

(a) 10 µm

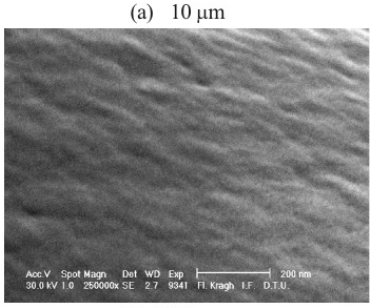

(b) 200 nm

Fig.2 Hydrophilic polystyrene particles with hydroxyl groups on their surfaces. Particle diameter 30 µm[21]

The significance of particle size, shape and surface character was approached by Marschall et al.[21] who showed that when globally spherical particles, hydrophobic as well as hydrophilic ones, with very smooth surfaces, Fig.2, were seeded into filtered tap water passing through a Keller vortex-flow nozzle, a tensile strength of the water considerably above the level set by vapour cavities (or perfectly hydrophobic solid spheres) of size as the particles was achieved. The remaining natural particles were of size <1 µm and gave the water an ultimate tensile strength of ~0.13 MPa (as that of 2.2 µm diameter vapour cavities), but smooth spherical particles of diameter 3µm, and thus 3 times the largest natural ones, were unable to provoke cavitation. Notably larger smooth spherical particles (diameters from 20 µm to 76 µm) did cause cavitation, but at tensile stress levels 5-10 times higher than vapour cavities of size as the particles. Thus, cavitation nuclei on the particle surfaces, much smaller than the particles themselves were responsible for the tensile strength. Expectedly, surfactant molecules in the tap water used for the flow system have allowed the development of surface nanobubbles at shallow, nano-size surface irregularities, Fig.2(b). These may have merged during exposure to tensile stress in the flow system so that critical interfacial nuclei of radius up to a few micrometer developed, as demanded for the measured tensile strengths of ~0.05 MPa to ~0.09 MPa.

Spherical 30 µm diameter particles from the same batch (supplied in liquid suspension) as used by Marschall et al. were later used by Arora et al.[22] for cavitation experiments in stationary Milli-Q water, applying a lithotripter for the production of strong stress pulses, each of duration ~10µs and having a compressive front followed by a tensile trailing wave Fig.3. Here even a ~7 MPa tensile stress pulse (which makes a vapour cavity of radius ~0.02 µm explode!) could not provoke cavitation. This might be a consequence of the Milli-Q water being so clean that cavitation nuclei were not developed.

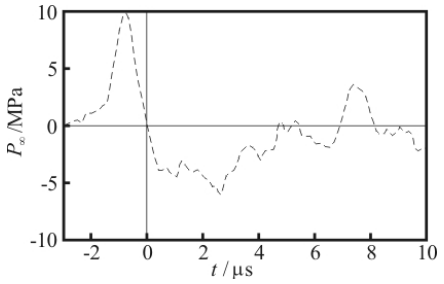

Fig.3 Lithotripter pressure pulse in Milli-Q water without particles[23]

However, it seems as likely that the leading compressive part of the lithotripter pulse, having a peak strength ~10 MPa and a duration of 1µs -2 µs, reduced the size or even eliminated the interfacial cavitation nuclei, thus preventing inception at these particles. To obtain cavitation with the lithotripter pulse Arora et al. therefore shifted to using almost spherical particles (of mixed diameters 30 µm -150 µm) that had a rough surface, Fig.4. With these particles, inception occurred at a tensile stress of ~2.5 MPa, corresponding to vapour cavities of diameter 0.06 µm. These particles were stored dry, and at atmospheric conditions until being used, and thus they were hardly free of contamination.

Beyond doubt, at tensile stress in a flow system these rough spherical particles would have given the water a relatively low tensile strength, as even the smooth spherical particles did in Marschall et al's experiments. However, the strong compressive front of the lithotripter pulse acceptably explains that the interfacial cavitation nuclei were strongly reduced in

size before the arrival of the tensile wave, thus causing the high tensile strength observed.

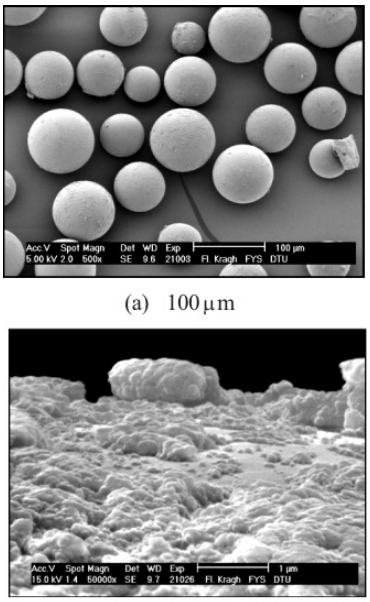

Fig.4 30 μm -150 μm diameter polystyrene particles with corrugated surfaces[22]

Unfortunately interfacial cavitation nuclei are so small that they cannot be observed by optical microscopy for which the wavelength of light sets a resolution limit of about 0.5 μm. However, the modern techniques available for studying solid surfaces, Scanning Tunnelling Microscopy (STM) and Atomic Force Microscopy (AFM), offer a possibility of studying nano-voids at solid-water interfaces, i.e., cavitation nuclei. The detection of nano-voids by use of STM presupposes that when the submerged STM-tip meets a void, the tunnelling barrier is smaller along the cavity surface than if the tip moves on to the drained solid surface below, while the use of AFM presupposes that the liquid-gas interface of a void can supply a detectable force on the AFM-tip. Otherwise the tip will ignore the void, and only the solid surface below is detected.

Actually, shortly after the STM technique was developed, specimen surfaces of gold (Au) that was vapour-deposited onto a lacquered aluminium substrate, specimen surfaces of titanium nitride (TiN) that was deposited onto a tungsten (W) substrate, and specimen surfaces of W were studied in air as well as in water[18,24,25], and it was revealed that their surface topographies appeared notably more smooth in water than in air, Fig.5, when scanned with sharp STM tips made from W. This was a first indication, that interfacial voids are present in large numbers at the fine roughness structures of submerged solid surfaces, of lateral dimensions up to about 200 nm, and that STM could be used to reveal their existence. But how could this imaging be achieved by STM? And could interfacial voids be observed by other techniques?

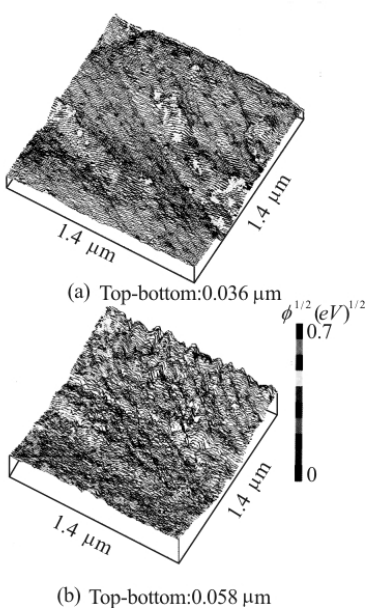

Fig.5 The same element of the surface of a W-specimen recorded (a) when submerged in water, and (b) subsequently in air. We notice the apparent smoothness of the surface in water compared with that in air. Also the tunnelling barrier signal is lower in air than in water because in air the tip is extremely close to the specimen surface[24]

In atmospheric air as well as in water W-surfaces oxidize immediately. Therefore the W-tips and W-specimens used in the experiments were covered with oxide layers of very low conductivity. Likewise, the surface of the TiN depositions consisted of TiO_2, which is also non-conductive. The immediate expectation would be that the insulating surface layers would make scanning tunnelling microscopy impossible. However, in atmospheric air, a mono-layer of water molecules (van der Waals diameter 2.8 Å) is adsorbed to most solid surfaces, and in the experiments a sufficient transfer of electrons for a small tunnelling current (4 nA) seems achieved by electron transfer along such adsorbed water mono-layers, the layers on the oxidized tip and specimen being so close that they have merged to give the remarkably low tunnelling barrier signals measured by vibrating the STM-tip perpendicular to the surface during topographic scanning in air, $0(eV)^{1/2} < \Phi < 0.3(eV)^{1/2}$. This explains that the topography of insulating specimen surfaces could be recorded using STM in air. By STM in water a few interfacial layers of orderly structured water are formed at the tip surface as well as at the specimen surface, at least those in direct contact with the solids

being solid-like. Also at the water-gas interface of a void an orderly structured layer of water molecules forms, though less stable. By STM in water these interface layers have eased the electron transfer compared to that obtained in air, and likewise the orderly structure of the interface layer of water at the surface of a gas bubble explains that the recording of void surfaces was possible, the tunnelling barrier signals at void surfaces being the same as at solid surfaces, and equal to those measured in bulk water, $0.5\ (eV)^{1/2} < \Phi < 0.7\ (eV)^{1/2}$. Thus, the eased electron transfer in water has allowed a slightly larger tunnelling gap (tip-specimen distance) than in air, allowing the orderly structured layers of water on the tip and specimen to be separated by bulk water. STM apparently allows the recording of even very small interfacial voids because the tip does not make contact to their surface. From Fig.5 we notice that the fine scale roughness structures visible in air (Fig.5(b)) are absent in water (Fig.5(a)), leaving only the large scale grinding traces produced during the specimen preparation.

We can expect that when the temperature drops towards the freezing point the solid-like character of the interfacial water layers on a submerged solid surface gradually grows beyond the layer in direct contact with the solid surface, the more the lower the temperature. At convex surface locations the bending of such solid-like layers cause tensile stress in the outermost layer, which just destabilises its solid-like structure. At concave surface locations it is the water layer that bonds to the solid, which is strained. It may cause the water-solid bonds to break, thus producing an interfacial void[19]. This gives an explanation of why the tensile strength of water drops abruptly when the temperature approaches the freezing point[3,10].

The STM technique was soon supplemented by the AFM technique, and later studies of interfacial voids at submerged surfaces have focused on the use of this technique. At first AFM contact mode imaging was used for the study of interfacial voids[26]. It was found that when the AFM-tip approached the solid surface, and a void was present at the location investigated, then at tip-void contact a downwards directed surface tension force on the tip made it penetrate the void abruptly, until specimen contact was achieved, i.e., the void height/depth was recorded. On stainless steel surfaces interfacial voids of height up to ~60 nm were revealed by such snap-in of the tip, Fig.6. The tips used were made from Si_3N_4 and had a cone half-angle of 35°, which resulted in the surface tension force on the tip being downwards directed at tip-void contact, and it explains the rapid snap-in observed. Thus, the existence of interfacial voids was shown by AFM, but a topographic mapping was still lacking.

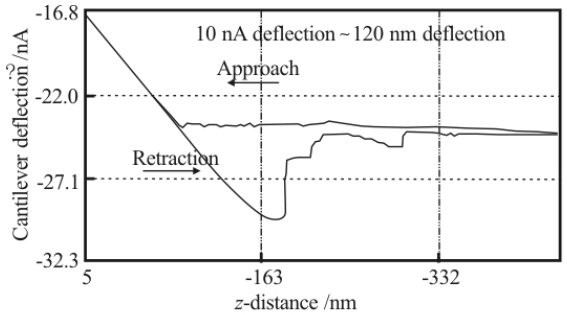

(a) AFM-spectroscopy at a water-stainless steel interface

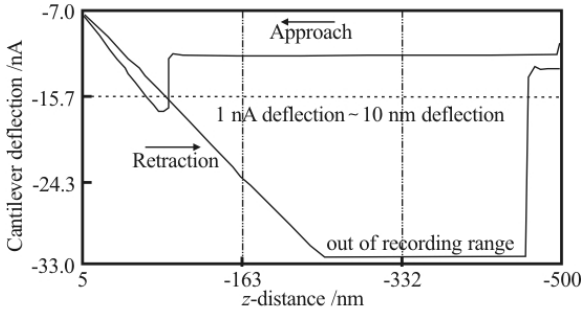

(b) AFM-spectroscopy at a void on awater-stainless steel interface

Fig.6 When in water a Si_3N_4 AFM tip approaches (a) a stainless steel surface there is only a small snap-in at contact ($z \approx -87$ nm), but at its retraction notable van der Waals forces between tip and specimen must be overcome by cantilever deflection before snap-out occurs ($z \approx -185$nm). b) At an interfacial void a strong snap-in corresponding to the void height (here ~60 nm) occurs. At tip retraction the van der Waals forces as well as the surface tension forces on the tip have to be overcome before snap-out occurs ($z \approx -455$nm)[26]

Later the development of highly hydrophilic silicon AFM-probes with a cone half-angle of only 10° allowed Holmberg et al.[27,28] to depict the interfacial voids topographically also by use of contact-mode AFM, because now the surface tension force was upwards directed when tip-void contact occurred. By vapour deposition of Au on mica substrates, atomically flat grain surfaces were obtained. When these were submerged in Milli-Q water, surface voids of diameters up to ~100 nm were observed on the grain surfaces, but the void heights recorded were only a few nanometer. Also crevices between the grain boundaries carried voids, and they were evidently much larger and of considerable depth, Fig.7. A simple theory of force balance for the tip-void interaction at the void centre was presented, but no analysis was made of how deeply the tip penetrated into the voids during scanning from one side of a void to the other. Certainly, the true centre heights of the voids were notably higher than revealed by the line scans shown, while the void diameters seem fairly correct. Voids of size below some lower

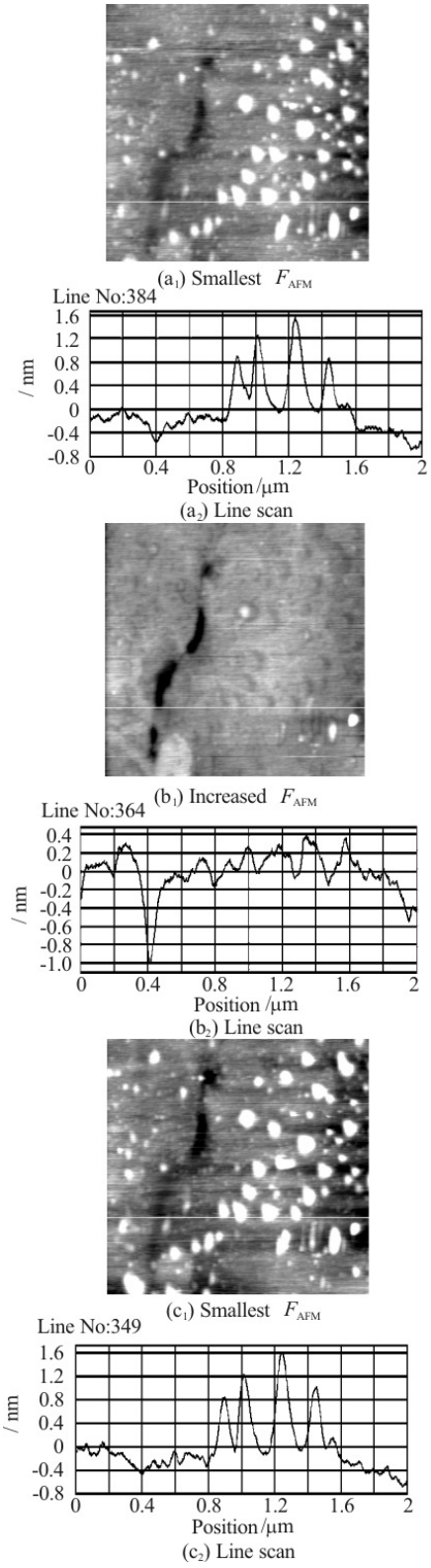

Fig.7 AFM image of a 2 μm × 2 μm gold specimen surface submerged in water and scanned in contact mode (a_1) with the smallest scanning force possible, (a_2) the line scan indicated in (a_1), (b_1) with an increased (normal) scanning force, (b_2) the line scan indicated in (b_1), (c_1) again with the smallest scanning force possible, (c_2) the line scan indicated in (c_1)[27]

limit have been unable to lift the tip from the sold surface. Milli-Q water was used, but the specimens had been exposed to atmospheric air before being submerged, and contamination by alien molecules has undoubtedly been a factor in the stabilisation of the surface nanovoids observed on the atomically flat Au-surfaces.

The alternative technique of tapping mode AFM was first used successfully by Lou et al.[29] for the recording of nanobubbles on mica and HOPG surfaces. In tapping mode the AFM tip oscillates at the cantilever resonance frequency, perpendicular to the investigated specimen surface. When in air the tip comes very close to a solid surface during its oscillation the attractive intermolecular force between the tip and the specimen grows strongly and tend to cause snap-in. However, the high-frequency oscillation of the cantilever allows the tip to escape the snap-in, but the resonance frequency is shifted, and a detectable amplitude and phase shift of the oscillation occurs. These shifts allow the topography of the solid surface to be recorded. In water the solid-solid interaction is partly screened by the water molecules, but the structured water layers adsorbed to the tip and specimen surfaces tend to merge, which supplies an attractive force that shifts the resonance frequency and phase. At a void surface the merging of its structured interface layer with that on the tip likewise causes an attractive force that shifts the resonance frequency and phase. This interpretation of tip-object interactions in water offers an explanation of why solid as well as void surfaces can be recorded by tapping mode AFM, and probably with very little disturbance of the void shape if only the parameters of operation are well chosen. The phase and topography images of a void presented by Holmberg[30] should be interpreted from such considerations.

Recently Borkent et al.[31] used AFM tapping mode for the study of surface nanobubbles on very smooth surfaces of polyamide (static contact angle 80°) and hydrophobized silicon (advancing contact angle ~100°) submerged in Milli-Q water. On all specimens studied, surface nanobubbles of diameters from 60 nm to 300 nm and of heights from 3 nm to 40 nm were observed with a number density of 10 per μm^2 to 80 per μm^2. We notice that the bubble heights recorded are much more realistic than those recorded by contact mode AFM. The attractive force between the structured water layers at the tip and bubble surfaces suggest that in AFM tapping mode the surface is slightly deformed, so that the measured heights are slightly too large. We also notice that a spherical cap with a height of 40 nm and an attachment radius of 150 nm has a radius of curvature of ~300 nm. If the undisturbed bubble height is smaller the bubble radius

is larger than 300nm. It corresponds closely to the size of the smallest free gas bubbles observed by Johnson and Cooke! Apparently, the number density of Borkent et al.'s surface bubbles was reduced if the specimen surfaces were flushed with ethanol immediately prior to being submerged, and if the specimens were brought from degassed ethanol into degassed water, surface bubbles were not at all formed. This observation supports that nanobubbles grow by diffusion of gas from the liquid phase into nucleation sites on the solid surface (maybe aided by resonance oscillations of the interfacial voids[19]), but it seems likely that surfactant molecules are essential for the stabilisation of the surface nanobubbles observed.

Borkent et al. also investigated the role of their surface nanobubbles in causing cavitation. When exposed to lithotripter pulses of peak tensile stress ~6 MPa, these bubbles did not cause cavitation - and the critical strength of the observed surface nanobubbles was estimated to be an order of size smaller. After the exposure to a lithotripter pulse the submerged surfaces were again investigated by AFM, and surprisingly the nanobubbles could still be observed on the specimen surface. However, cavitation did develop from microscopic cracks in the specimen surfaces, and also from occasional spots of contamination.

On this basis the authors characterized the survival of the surface nanobubbles to shock wave exposure as "superstability". However, no evidence was given for the response of the nanobubbles to the full lithotripter pulse during its passage, as the nanobubbles could be observed in the AFM only before and after the cavitation experiment was made – and a significant period of time passed when moving the specimen between the experimental equipments.

The strong compressive wave of ~7 MPa, leading the lithotripter pulse, has certainly reduced the size of the wall-attached surface nanobubbles dramatically, or it has eliminated them, thus raising their tensile strength beyond the tensile stress of 6 MPa available in the subsequent trailing wave of the pulse. Contrary, the liquid-gas interfaces of gaseous voids trapped in cracks essentially have reverted to their equilibrium state when the compressive pulse had passed, which explains that these voids were able to cause cavitation at the tensile stress that followed. These observations are also discussed in Section 3.2 of the present article. The above interpretation is in harmony with the observation that in Milli-Q water the very smooth particles in Fig.2 did not cavitate at exposure to lithotripter pulses with a trailing tensile stress of ~7 MPa , while those with irregular surface structures in Fig.4 did cavitate at ~2.5 MPa[22].

The AFM observations in Ref.[31], which show that after exposure to the lithotripter pulse the surface nanobubbles had their original size and shape, indicate that time is a decisive parameter. After exposure to the compressive part of the lithotripter pulse, surface conditions similar to those originally causing the formation of surface nanobubbles have probably characterized the surface, but local supersaturation of the liquid with gas from the collapsed bubbles in combination with the trailing tensile wave has led to re-formation of the nanobubbles after the pulse had passed. This is in harmony also with Harvey and Strasberg's observations that pressurisation increases the tensile strength of water after the excess pressure is released – but in their experiments the time scale of pressurization was very much longer than in Borkent et al.'s, and has led to diffusion balance in their systems.

The large difference of the tensile strength of water measured in lithotripter experiments and in flow experiments indicates that it might be advantageous to modify the lithotripter pulse to have a leading tensile wave, followed by a compressive trailing wave. This would allow the real tensile strength to be detected on-site with a lithotripter pulse, because the compressive pulse would not disturb the cavitation nuclei. In presently used systems for tensile strength measurement a sample of liquid is transferred to an external measuring system and, most probably, this causes significant changes of the cavitation nuclei, and thus of the tensile strength measured. A pulse reversal of the lithotripter pulses might be beneficial also in medical applications because much lower tensile stresses would produce the cavity clouds – and a smaller loading of the tissue exposed to the pulses would be achieved.

3. A recent model for cavitation nuclei

The experimental results of Johnson and Cooke[14] demonstrate that free gas bubbles can be stabilised by a skin, but experimental investigations have also shown that solid surfaces harbour cavitation nuclei in cracks and crevices, as suggested already by Harvey et al.[7], as well as on smooth surfaces[21-31]. Briggs[3] found that scrupulous cleanliness was decisive for obtaining a high tensile strength of water, and definitely, contamination of interfaces is a primary factor in modelling cavitation nuclei.

3.1 *Free gas bubbles*

Yount[12] assumes free gas bubbles to be stabilised by a skin of amphiphilic molecules (surface-active substances) that cover their surface. Recently the critical pressure of such skin-stabilised free gas bubbles as well as that of skin-stabilised gas bubbles attached to solid surfaces submerged in water saturated at the initial far-field pressure $p_{\infty,o}$ was calculated[32]. At the water-gas interface of the bubbles the hydrophilic heads of the amphiphilic

molecules bond to water molecules, while their hydrophobic tails bound the gas content of the bubbles, thus forming a skin on each bubble surface that allows the gas in the void to be in diffusion balance with that in solution. At equilibrium conditions the bubble surface of radius $R = R_o$ has an effective surface tension $\gamma_{eff,o} = 0$, which by Eq.(2) gives $p_{g,o} = p_{\infty,o} - p_v$. If the bubble is exposed to a rapid drop of the far field pressure $p_\infty(t)$ it expands to the time-dependent radius $R(t)$ and the skin of initial area A_o breaks into islands, separated by growing areas of water, $A_{H_2O}(t)$. At isothermal expansion $P_g(t)$ drops inversely proportional to the bubble volume $V(t)$, and thus

$$p_g(t) = \left(p_{\infty,o} - p_v\right)\frac{V_o}{V(t)} \tag{5}$$

The areas of water have the surface energy $\gamma_{H_2O} A_{H_2O}(t)$, but as the skin areas do not contribute to the surface energy of the bubble, its effective surface tension $\gamma_{eff}(t)$ is given by

$$\gamma_{H_2O} A_{H_2O}(t) = \gamma_{eff}(t)\left[A_{H_2O}(t) + A_o\right] \tag{6}$$

and during the bubble expansion the pressure jump across the bubble surface is given by

$$\Delta p = p_g(t) + p_v - p_\infty(t) = \frac{2\gamma_{eff}}{R(t)} \tag{7a}$$

which for a spherical free bubble results in

$$\Delta p = p_g(t) + p_v - p_\infty(t) = \frac{2\gamma_{H_2O}}{R(t)}\bullet$$

$$\left[1 - \left(\frac{R_o}{R(t)}\right)^2\right] \tag{7b}$$

Likewise Eq.(5) gives

$$p_g(t) = \left(p_{\infty,o} - p_v\right)\left[\frac{R_o}{R(t)}\right]^3$$

At the critical condition $\mathrm{d}\left(p_\infty(t) - p_v\right)/\mathrm{d}R(t) = 0$, which with Eq.(7b) leads to

$$\left(\frac{R_{crit}}{R_o}\right)^2 = 3\left[1 + \left(p_{\infty,o} - p_v\right)\frac{R_o}{2\gamma_{H_2O}}\right] \tag{8}$$

and

$$p_v - p_{\infty,crit} = \frac{4\gamma_{H_2O}}{3R_{crit}} \tag{9}$$

We notice that during bubble growth the elements of water have a radius of curvature different from $R(t)$, and thus the bubble is not perfectly spherical. Actually, some of the bubbles photographed by Johnson and Cooke[14] were not spherical. Eqs.(8) and (9) are identical with those describing critical conditions of gas bubbles without a skin. Thus, when a free gas bubble *is* covered by a skin, and it is in diffusion balance at the far field pressure $p_{\infty,o}$, the bubble responds to a tensile stress precisely as an ordinary free gas bubble with the same gas content, but the ordinary gas bubble has of course a smaller initial radius R_o, a higher initial gas pressure $p_{g,o}$, and it is not in diffusion balance. The skin results in a larger critical radius of the bubble and a numerically smaller critical pressure than found for ordinary gas bubbles, but the influence of the skin is not at all dramatic – it primarily makes stabilisation of the gas bubble possible.

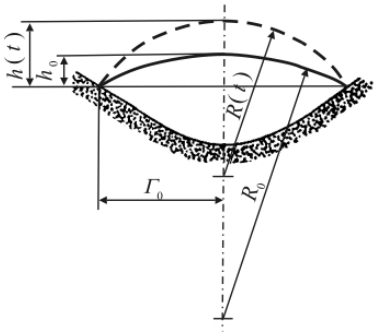

Fig.8 Submerged solid surface that has a concave element from which the water has detached, thus forming an interfacial void. The void surface is shown at initial conditions, (R_o, h_o), and during its subsequent expansion, ($R(t), h(t)$), driven by reduction of the far field pressure[32]

3.2 *Interfacial gas bubbles*

Solid surfaces submerged in a liquid tend to adsorp amphiphilic molecules. We can expect that

clusters of such molecules form weak spots, and that these are the basis for the development of interfacial gas bubbles. Thus Eqs. (5)-(7a) are valid not only for free gas bubbles, but also for gaseous voids at solid-liquid interfaces. For calculation of the critical pressure of a skin-covered interfacial gas bubble we assume that a spherical cap of contact radius Γ_o and height h_o defines the cap-volume $V_{sph,o}$, while the volume V_s of gas beneath it depends on the geometry of the solid surface, Fig.8.

For time $t \le 0$ the void volume

$$V_o = V_s + V_{sph,o} = V_s + \frac{\pi}{6} h_o (3\Gamma_o^{\,2} + h_o^{\,2}) = V_s + \pi h_o^{\,2} (R_o - \frac{h_o}{3}) \qquad (10)$$

in which $R_o = (\Gamma_o^{\,2} + h_o^{\,2}) / (2h_o)$, and with the void being in diffusion balance the saturation pressure $p_{g,o} = p_{\infty,o} - p_v$.

At $t = 0$ the far field pressure drops to $p_\infty(t) < p_{\infty,o}$, and the spherical cap of initial area A_o expands into a two component cap of area $A(t)$, composed of elements of skin as well as of water. Γ_o remains constant, because a change of the contact radius requires the molecular bonds to break at the liquid-solid interface, and it takes time. Thus, $R_o \to R(t)$, $h_o \to h(t)$ and $V_o \to V(t)$ while the gas pressure is given by Eq.(5).

The expanding spherical cap of area

$$A(t) = 2\pi R(t) h(t) = \pi \left[\Gamma_o^{\,2} + h(t)^2 \right]$$

acquires an effective surface tension

$$\gamma_{eff} = \gamma_{H_2O} \frac{h(t)^2 - h_o^{\,2}}{\Gamma_o^{\,2} + h(t)^2} \qquad (11)$$

Further, the force balance, Eq.(7a), requires

$$p_v + p_g(t) - p_\infty(t) = 4\gamma_{H_2O} \bullet \frac{h(t)\left[h(t)^2 - h_o^{\,2} \right]}{\left[\Gamma_o^{\,2} + h(t)^2 \right]^2} \qquad (12)$$

or with Eq.(5)

$$\left[p_\infty(t) - p_v \right]^* = \frac{6V_s^* + \pi h_o^* \left(1 + h_o^{*2}\right)}{6V_s^* + \pi h(t)^* \left[1 + h(t)^{*2} \right]} - \frac{4\gamma_{H_2O}}{(p_{\infty,o} - p_v)\Gamma_o} \frac{h(t)^* \left[h(t)^{*2} - h_o^{*2} \right]}{\left[1 + h(t)^{*2} \right]^2} \qquad (13)$$

in which

$$\left[p_\infty(t) - p_v \right]^* = \frac{\left[p_\infty(t) - p_v \right]}{(p_{\infty,o} - p_v)}, \quad V_s^* = \frac{V}{\Gamma_o^{\,3}},$$

$$h_o^* = \frac{h_o}{\Gamma_o}, \quad h(t)^* = \frac{h(t)}{\Gamma_o}$$

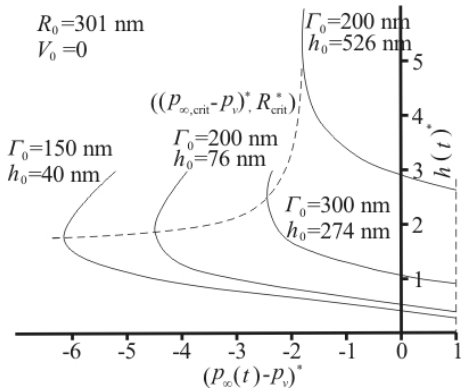

Fig.9 Four cases of growth for surface nanobubbles on a planar surface submerged in water at exposure to simple tensile stress. In all the cases the initial equilibrium radius of curvature is taken to be R_o = 301nm at standard temperature and pressure ($[p_\infty(t) - p_v]^* = 1$) while the bubble contact radius Γ_o and its height h_o varies from case to case. Γ_o = 150nm, h_o = 40nm represents the largest surface nanobubbles reported in Ref.[31]

Equation (13) allows us to calculate the bubble growth due to reduction of the far field pressure, i.e., the relationship $h(t)^*$ vs. $\left[p_\infty(t) - p_v \right]^*$. In Fig.9 examples are shown based on the surface nanobubbles observed by Borkent et al.[31] for which $V_s \approx 0$, and thus $V_o = V_{sph,o}$. The largest of these bubbles were reported to have Γ_o = 150nm and h_o = 40nm, which gives $R_o \approx$ 301nm, and we take this radius as characteristic of the family of surface nanobubbles observed. We may imagine that by time new

surface-active molecules can be supplied to the bubble surface without changing R_o, and then Γ_o and h_o grow until ultimately $h_o = 2R_o$ and $\Gamma_o = 0$. In this case Eq.(12) reduces to Eq.(7b), and the surface nanobubble transforms into a free spherical gas bubble. This might be a mechanism of formation of skin-covered free gas bubbles in water.

Critical conditions for a surface nanobubble are achieved when

$$\frac{\mathrm{d}\left[p_\infty(t) - p_v\right]}{\mathrm{d}h(t)} = \frac{\mathrm{d}\left[p_g(t)\right]}{\mathrm{d}h(t)} -$$

$$\{4\gamma_{\mathrm{H_2O}}\{\Gamma_o{}^2[3h(t)^2 - h_o{}^2] - h(t)^2 \bullet$$

$$[h(t)^2 - 3h_o{}^2]\}\}/[\Gamma_o{}^2 + h(t)^2]^3 \qquad (14)$$

With Eqs.(5) and (9) we obtain

$$\frac{6V_s^* + \pi h_o^*\left(3 + h_o^{*2}\right)}{\left[6V_s^* + \pi h_{crit}^*\left(3 + h_{crit}^*{}^2\right)\right]^2} =$$

$$\frac{4\gamma_{\mathrm{H_2O}}\left[h_{crit}^*{}^4 - 3h_{crit}^*{}^2\left(1 + h_o^{*2}\right) + h_o^{*2}\right]}{3\pi\left(p_{\infty,o} - p_v\right)\Gamma_o\left(1 + h_{crit}^*{}^2\right)^4} \qquad (15)$$

which for given initial void data allows us to calculate h_{crit}, and with

$$R_{crit} = \frac{\Gamma_o{}^2 + h_{crit}{}^2}{2h_{crit}}$$

and Eq.(12) we can determine $p_{\infty,crit} - p_v$. We notice that for a full spherical gas bubble in contact with a planar solid surface, $V_s = 0$ and $h_o = 2R_o$, $\Gamma_o = 0$, Eq.(15) reduces to Eq.(8).

For the largest surface nanobubbles observed in Ref.[31] ($V_s = 0$, Γ_o = 150nm, h_o = 40nm, i.e., $R_o \approx$ 301nm) Eq.(15) gives h_{crit} = 272nm and R_{crit} = 177nm, while Eq.(13) gives

$$p_{\infty,crit} - p_v \approx -0.61 \text{ MPa}$$

Thus, a normal tensile stress pulse an order of magnitude weaker than that actually applied by the lithotripter pulse would have caused the largest surface nanobubbles to cavitate (as also estimated by the authors), but apparently the leading compressive part of this pulse severely influences the inception conditions.

It is notable that all of Johnson and Cooke's skin-covered free gas bubbles collapsed when the pressure was raised from atmospheric conditions to an excess pressure of only 0.0138 MPa. This suggests that Borkent at al.'s surface nanobubbles collapsed at exposure to the 7.0 MPa pressure rise at the front of the lithotripter pulse. Expectedly, the compression has made their bubble caps shrink from the rim towards the bubble centre, leaving their skin on the solid surface, while their gas content was concentrated inside ordinary, hemispherical, attached bubbles that reached a minimum radius $R_{\min}$, determined by the far field peak pressure $p_{\infty,\max}$, and caused a Laplace pressure $2\gamma_{\mathrm{H_2O}} / R_{\min}$. If we neglect diffusion of gas from the bubbles to the liquid during collapse, caps of initial volume $V_{sph,o} = \pi h_o\left(3\Gamma_o{}^2 + h_o{}^2\right)/6$ have transformed into hemispherical attached bubbles of a radius $R_{\min}$, governed by

$$p_{\infty,\max} - p_v + \frac{2\gamma_{\mathrm{H_2O}}}{R_{\min}} = \left(p_{\infty,o} - p_v\right)h_o \bullet$$

$$\frac{3\Gamma_o{}^2 + h_o{}^2}{4R_{\min}{}^3} \qquad (16)$$

For the largest of the surface nanobubbles in Ref.[31] the compressive wave of $p_{\infty,\max} \approx 7.0$MPa leads to $R_{\min} \approx 16$nm. This radius is so small that surface tension makes the pressure inside the bubbles come up to ~17 MPa, and actually, diffusion of gas from the bubbles into the liquid cannot be neglected. Therefore, the bubbles have shrunk much further, most probably causing their total elimination before the arrival of the tensile stress wave. However, the gas from the collapsed bubbles has locally supersaturated the liquid, and after the pulse passage the skin left on the solid surface has allowed the surface nanobubbles to re-develop by diffusion of gas molecules into the interfacial structures. Thus, the above calculations are in harmony with Borkent at al.'s observation that surface nanobubbles do not cause cavitation at exposure to lithotripter pulses. However, at surface cracks cavitation was observed, but here the physics of the bubble compression is different.

Let us model what happens at a crack by considering a bubble cap with a skin, of contact radius

Γ_o and height h_o which just covers a gas filled cylindrical hole of depth L_o in a solid surface. The compressive front of the lithotripter pulse makes the liquid move as a piston into the hole, compressing the gas. In this case surface tension forces do not increase the gas pressure the bubble, and when the far field pressure drops, the bubble surface moves out again. Neglecting diffusion and for simplicity also damage to the skin, the solid wall of the hole allows the bubble to revert essentially to its initial conditions when the expansive trailing wave arrives, and thus

$$V_o = 4\pi L_o \Gamma_o^{\,2} + \frac{\pi h_o \left(3\Gamma_o^{\,2} + h_o^{\,2}\right)}{6}$$

If as an example we choose $\Gamma_o = 150$nm, $h_o = 40$nm and $L_o = 2\Gamma_o$, Eq.(15) gives $h_{crit} = 278$nm, $R_{crit} = 180$nm and $p_{\infty,crit} - p_v \approx -0.55$ MPa. Actually, the crack depth is of minor importance, and if in the example calculated we let $L_o \to \infty$ we find $h_{crit} = 268$nm, $R_{crit} = 176$nm and $p_{\infty,crit} - p_v \approx -0.53$ MPa. Though no details are given in Ref.[31] about the crack dimensions this model explains why Borkent et al. observed cavitation to occur at cracks in the solid surfaces though their surface nanobubbles appeared stable to the lithotripter pulses.

If we let the volume V_s increase the gas pressure $p_g(t)$ in the bubble becomes relatively less sensitive to the expansion of the bubble surface, and for sufficiently large V_s even positive values of the critical pressure $p_{\infty,crit} - p_v$ become possible.

By example, let us for simplicity take $h_o = 0$ and (though not realistic for interfacial voids) let $V_s \to \infty$. Now by Eq. (15) $h_{crit}^{*\,2} = 3$ and the equation of bubble growth, Eq.(13), gives the lower limit of bubble size $\Gamma_{o,inf}$ at which a positive critical pressure can occur

$$\Gamma_{o,inf} = \frac{3\sqrt{3}}{4} \frac{\gamma_{\mathrm{H_2O}}}{p_{\infty,o} - p_v}$$

For water at standard temperature and pressure we get $\Gamma_{o,inf} > 1\times10^{-6}$ m. Thus rough surfaces, and in particular surfaces with cracks, may cause interfacial voids to reach critical size already when the far field pressure approaches zero through positive values. We notice, that the quantity V_s in Eqs.(13) and (15) represents the gas content required for setting up the pressure in the bubble, but this gas content may arise as well by diffusion of gas into the bubble cap when the liquid turns supersaturated relative to the bubble at pressure reduction.

4. Cavitation scale effects in model tests

The prediction of cavitation on prototype objects is usually based on model tests, and in this context scale effects are decisive. Here the Thoma number

$$\sigma = \frac{P_\infty - p_v}{\frac{1}{2}\rho U_\infty^{\,2}} \tag{17}$$

in which P_∞ and U_∞ are the pressure and velocity upstream of the object is a key parameter. In different model tests with a specific body as well as in prototype experiments with a given body shape, cavitation inception is expected to occur at a characteristic value of σ. However, the water quality - the tensile strength of water - has until recently completely confused such experiments, making results obtained with different test facilities incomparable, and also different from prototype results. However, by correcting for the tensile strength of the water an empirical scaling law for incipient cavitation was found by Keller[33-35]. The cavitation inception number σ_i was found to depend on a characteristic length L of the object, on U_∞, and on the viscosity ν of the liquid according to the empirical relation

$$\sigma_i = K_0 L^{1/2} \left(\frac{\nu_0}{\nu}\right)^{1/4} \left[1 + \left(\frac{U_\infty}{U_0}\right)^2\right] \left(1 + \frac{K_0 S}{4}\right) \tag{18}$$

in which the shape factor K_0 is an experimentally determined quantity characteristic for each specific body shape. S is the standard uncertainty of the free flow velocity induced by turbulence generators, ν_0 is the kinematic viscosity of water at 20°C, while U_0 is a basic velocity (≈12 m/s).

Keller's formula presupposes that correction is made for deviations from zero tensile strength of the water, but actually, Eq.(18) itself seems influenced by the cavitation nuclei, which are extremely sensitive to changes of the physical conditions. Keller measured the tensile strength of water samples taken repeatedly at a position upstream of the object being studied. However, in Keller's closed water tunnel the cavitation nuclei were maybe in diffusion balance at the saturation pressure of the water when they approached the tunnel contraction, but when shortly later they arrived at the position of measurement for

velocity, pressure and tensile strength in the test section, they had experienced a pressure drop of $\sim 1/2\rho U_\infty{}^2$, and diffusion of gas into the expanded nuclei was in progress. This continued after the water had passed the section of measurement on its way to and past the object. Also, the nuclei in the samples of water being transferred to the equipment used for tensile strength measurement must have changed their gas content during the process of transfer and measurement. Thus, the gas content of the cavitation nuclei has increased in the tunnel flow after passage of the point of sampling as well as in the water samples taken out for measurement. The velocity term in Eq.(18) seems a consequence of these changes.

Likewise, the dependency of the cavitation inception number on the object dimension L seems related to diffusion of gas into the cavitation nuclei. At given U_∞ the time of passage along the object contour grows proportionally to the body size. However, the rate of release of gas molecules from the liquid at bubble expansion drops by time due to the gradual reduction of the gas tension in the liquid phase near to the surface of the bubbles. It may explain the $L^{1/2}$ dependency in Eq.(18). We can expect also that an increase of the viscosity obstructs gas release into the bubbles, and that increase of the degree of turbulence promotes it.

The above interpretation of Eq.(18) suggests supplementary experimental research. First, a lithotripter with weak leading tensile stress pulse seems ideal for tensile strength measurement on-site at the location where Keller took out test samples of water. This will eliminate influence of the equipment for tensile strength measurement on the result, leaving only scale effects related directly to the flow between the location of measurement and the object. It is also worthwhile to notice that in contrast to cavitation tunnel experiments, experiments in towing tanks and in the ocean take place with the cavitation nuclei being in diffusion balance at the position of tensile strength measurement upstream of the object. This probably affects the scaling relations notably.

5. Conclusions

The model of cavitation nuclei considered in the present article is based on experimental results from a century of world-wide research, interpreted in the light of the conditions at which the experiments were carried out. This model successfully explains why the tensile strength of water can range from zero to hundreds of bar, and it links cavitation nuclei at solid surfaces (gas bubbles in cracks and surface bubbles) to free gas bubbles. However, the diffusion of gas into cavitation nuclei remains to be included. The major problem in understanding cavitation nuclei has been their stabilisation. Harvey et al.'s model[7] of interfacial nuclei at surface cracks as well as Fox and Herzfeld's skin model[11] for free gas bubbles were excellent first approaches to models describing cavitation nuclei, and remain basic ones. Briggs' observation[3] that scrupulous cleanliness is the decisive factor in achieving a high tensile strength has proved a key to the progress achieved. However, we still lack insight into skins that stabilise cavitation nuclei.

The new techniques, scanning tunnelling microscopy and atomic force microscopy, have proved able to visualise interfacial gas bubbles, and the present article presents interpretations of the modus operandi of these techniques in relation to interfacial voids.

The low tensile strength of water measured in flow systems at exposure to tensile stress and the high values observed when lithotripter pulses are used can be explained by the compression-tension shape of the lithotripter pulses used today. A reversed pulse shape in lithotripters is expected to prevent changes of the cavitation nuclei prior to producing cavitation with such generators. This may improve lithotripters for medical purposes and can lead to the development of a technique for on-site measurement of the tensile strength of water. On-site measurements would be valuable for studies of cavitation scaling laws for model tests and prototype experiments.

References

[1] FISHER J. C. The fracture of liquids[J]. **J. Applied Physics,** 1948, 19: 1062-1067.

[2] ZHENG Q., DURBEN D. J. and WOLF G. H. et al. Liquids at large negative pressures: Water at the homogeneous nucleation limit[J]. **Science,** 1991, 254: 829-832.

[3] BRIGGS L. J. Limiting negative pressure in water[J]. **J. Applied Physics,** 1950, 21: 721-722.

[4] BRENNEN C. E. **Cavitation and bubble dynamics**[M]. Oxford, UK: Oxford University Press, 1995.

[5] MØRCH K. A. **Dynamics of cavitation bubbles and cavitating liquid**[M]. In Erosion – A treatise on materials science and technology. USA: Academic Press, 1979, 16.

[6] EPSTEIN P. S., PLESSET M. S. On the stability of gas bubbles in liquid-gas solutions[J]. **J. Chemical Physics,** 1950, 18: 1505-1509.

[7] HARVEY E. N., BARNES D. K. and Mc ELROY W. D. et al. Bubble formation in animals[J]. **J. Cellular and Comparative Physiology,** 1944, 24: 1 -22.

[8] STRASBERG M. Onset of ultrasonic cavitation in tap water[J]. **J. Acoustical Society of America,** 1959, 31: 163-176.

[9] BARGER J. E. Thresholds of acoustic cavitation[R]. Tech. memorandum No. 57. Acoustics Research Lab. Harvard Univ., 1964, ONR Contract 1866 (24).

[10] KELLER A. P. Schlussbericht über das forschungs-vorhaben “beginnende kavitation, zugspannungen in flüssigkeiten” 2[R]. Teil , p.15. Oskar von Miller-Institut, Germany: Technischen Universität München/Obernach, 1982.

[11] FOX F. E., HERZFELD K. F. Gas bubbles with organic skin as cavitation nuclei[J]. **J. Acoustical Society of America,** 1954, 26: 984-989.

[12] YOUNT D. E. Skins of varying permeability: A stabilization mechanism for gas cavitation nuclei[J]. **J. Acoustical Society of America,** 1979, 65(6): 1429-1439.

[13] YOUNT D. E. On the elastic properties of the interfaces that stabilize gas cavitation nuclei[J]. **J. Colloid and Interface Science,** 1997, 193: 50-59.

[14] JOHNSON B. D., COOKE R. C. Generation of stabilized microbubbles in seawater[J]. **Science,** 1981, 213: 209-211.

[15] YOUNT D. E., GILLARY E. W. and HOFFMAN D. C. A microscopic investigation of bubble formation nuclei[J]. **J. Acoustical Society of America,** 1984, 76: 1511-1521.

[16] SIROTYUK M. G. Stabilization of gas bubbles in water[J]. **Soviet Physics – Acoustics,** 1970, 16: 237-240.

[17] GREENSPAN M., TSCIEGG C. E. Radiation-induced acoustic cavitation. Apparatus and some results[J]. **J. Research of the National Bureau of Standards – C.**, 1967, 71C: 299-312.

[18] MØRCH K. A., SONG J. P. Cavitation nuclei at solid-liquid interfaces[C]. **Cavitation – Proc. Institution of Mechanical Engineers.** UK: Int. Conf. Cambridge, 1992, Paper C453/059: 1-7.

[19] MØRCH K. A. Cavitation nuclei and bubble formation – a dynamic liquid-solid interface problem[J]. **J. Fluids Engineering, ASME,** 2000, 122: 494-498.

[20] CRUM L. A. Tensile strength of water[J]. **Nature,** 1979, 278: 148-149.

[21] MARSCHALL H. B., MØRCH K. A. and KELLER A. P. et al. Cavitation inception by almost spherical solid particles in water[J]. **Physics of Fluids,** 2003, 15: 545-553.

[22] ARORA M., OHL C. D. and MØRCH K. A. Cavitation inception on microparticles: A self-propelled particle accelerator[J]. **Physical Review Letters,** 2004, 92: 17450: 4.

[23] BORKENT B., ARORA M. and OHL C. D. et al. The acceleration of solid particles subjected to cavitation nucleation[J]. **J. Fluid Mechanics,** 2008, 610: 157-182.

[24] SONG J. P., MØRCH K. A. and CARNEIRO K. et al. STM investigations of solid surfaces in water and air[J]. **Surface Science,** 1993, 296: 299-309.

[25] SONG J. P., MØRCH K. A. and CARNEIRO K. et al. Investigation of scanning tunneling barrier signals in air and water[J]. **J. Vacuum Science and Technology B,** 1994, 12(3): 2237-2242.

[26] MORTENSEN N. A., KÜHLE A. and MØRCH K. A. Interfacial tension in water at solid surfaces[C]. **Third International Symposium on Cavitation.** Grenoble, France, 1998, 1: 87-91.

[27] HOLMBERG M., KÜHLE A. and GARNES J. et al. Cavitation nuclei at water-gold interfaces[C]. **Fifth International Symposium on Cavitation.** Osaka, Japan, 2003, Cav03-GS-1-001.

[28] HOLMBERG M., KÜHLE A. and GARNES J. et al. Nanobubble trouble on gold surfaces[J]. **Langmuir,** 2003, 19: 10510-10513.

[29] LOU S. T, OUYANG Z. Q. and ZHANG Y. et al. Nanobubbles on solid surfaces imaged by atomic force microscopy[J]. **J. Vacuum Science and Technology B,** 2000, 18(5): 2573-2575.

[30] HOLMBERG M. Organic and biological molecular layers on functionalysed sensor surfaces studied with atomic force microscopy[D]. Ph. D. Thesis, Copenhagen, Denmark: Technical University of Denmark, 2003.

[31] BORKENT B., DAMMER S. M. and SCHÖNHERR H. et al. Superstability of surface nanobubbles[J]. **Physical Review Letters,** 2007, 98: 204502(4).

[32] MØRCH K. A. Reflections on cavitation nuclei in water[J]. **Physics of Fluids,** 2007, 19: 072104: 4.

[33] KELLER A. P. New scaling laws for hydrodynamic cavitation inception[C]. **Second International Symp. on Cavitation.** Tokyo, Japan, 1994.

[34] KELLER A. P., ROTT H. K. The effect of flow turbulence on cavitation inception[C]. **ASME Fluids Engineering Division Summer Meeting.** Vancouver, 1997.

[35] KELLER A. P., ROTT H. K. Scale effects on tip vortex cavitation inception[C]. **1999 ASME/JSME Fluids Engineering Symposium on Cavitation Inception.** San Francisco,USA, 1999.